Meridional movement of wind anomalies during ENSO events and their role in event termination

Shayne McGregor[1,2], Nandini Ramesh[1], Paul Spence[1,2], Matthew H. England[1,2], Michael J. McPhaden[3] and Agus Santoso[1,2]

[1] Climate Change Research Centre, University of New South Wales, Sydney, Australia.

[2] ARC Centre of Excellence for Climate System Science, University of New South Wales, Sydney, Australia.

[3] NOAA/Pacific Marine Environmental Laboratory, Seattle, Washington, U.S.A.

Abstract

Observational analysis has shown that when El Niño Southern Oscillation (ENSO) events typically reach their peak amplitude in boreal winter the associated zonal wind anomalies abruptly shift southward so that the maximum anomalous zonal wind is located around 5°-7°S. Here, an analysis utilizing multiple wind products identifies a clear ENSO phase non-linearity in the extent of this meridional wind movement and its dynamically linked changes in equatorial heat content. It is shown that the meridional wind movement and its discharging effect increase with increasing El Niño amplitude, while both remain relatively small regardless of La Niña amplitude. This result implies that asymmetries in the extent of the meridional wind shift may contribute to the observed asymmetry in the duration of El Niño and La Niña events. We also evaluate the result sensitivities to wind product selection, and discuss Eastern Pacific (EP) and Central Pacific (CP) El Niño event differences.

1. Introduction

The tropical Pacific Ocean is home to Earth's largest source of interannual climate variability: the El Niño-Southern Oscillation (ENSO). Our understanding of the dynamics and oscillatory nature of ENSO has significantly increased over the last three decades, as illustrated by the success of theories such as the Recharge/Discharge Oscillator paradigm (RDO) of *Jin* [1997]. The RDO theory proposes that the poleward transport of equatorial

region warm near-surface waters during El Niño events discharges warm water volume (WWV) from the equatorial region, setting up conditions favorable for the termination of ENSO warm events. The basic principles of the RDO theory have been substantiated through the observational analyses of *Meinen and McPhaden* [2000] (hereafter MM2000). Furthermore, they show that variations in the equatorial region WWV are well represented by the second Empirical Orthogonal Function (EOF) of 20°C isotherm depth.

The original RDO theory was formulated in a simple linear conceptual framework and did not account for some subtleties of the ENSO cycle, such as: i) the apparent synchronization of ENSO events to the seasonal cycle [*Stein et al.* 2011]; ii) asymmetries in the duration of El Niño and La Niña [*Okumura and Deser* 2010]; and iii) the southward shift of zonal wind anomalies around the peak of ENSO events [*Harrison* 1987]. In this study we focus on this southward wind shift as it is likely also linked to the first two subtleties mentioned above.

To date, numerous studies have indicated that the meridional wind movement plays a role in the termination of ENSO events [e.g., *Harrison and Vecchi* 1999; *Vecchi and Harrison* 2003, 2006; *Lengaigne et al.,* 2006]. More recently, *McGregor et al.* [2012] using ERA-40 wind stresses over the period 1958-2001 suggested that the wind shift accounts for roughly half of the Pacific Ocean's WWV variability, while also highlighting its prominent role in the termination of Eastern Pacific (EP) El Niño events. It was noted that this meridional wind movement plays a much smaller role in Central Pacific (CP) events, also referred to as Warm Pool (WP) or Modoki type El Niño's [*Ashok et al*., 2007; *Kao and Yu* 2009; *Kug et al.*, 2009]

In light of the large differences seen across observational wind products [e.g., *Wittenberg* 2004], it is important to assess the sensitivity of *McGregor et al.*'s [2012] results to different choices of wind product. Here we focus on the more recent period of 1979-2008 for greater availability of products, and extend our analysis to the La Niña phase of the ENSO cycle. Our study supports the results of *McGregor et al.* [2012], confirming that the meridional wind shift plays a prominent role in the changes in equatorial WWV. An El Niño and La Niña

asymmetry in the wind shift, which has been previously linked to asymmetry in event duration [*Ohba and Ueda* 2009; *Okumura et al.,* 2011], emerges as a robust feature in our analysis. We further show that the extent of the wind shift is significantly and linearly related to changes in equatorial heat content. This pronounced correlation signifies the role of discharge and recharge of Pacific Ocean heat content on the observed asymmetry in ENSO duration via meridional wind movements.

2. Data

In this study monthly mean wind data from all known available global wind products that span the period 1979-2008 are utilized. These are the ECMWF interim reanalysis [ERA-interim; Dee and Uppala 2009], the Japanese reanalysis [JRA; *Onogi et al*., 2007], the NCEP/NCAR reanalysis 1 [NCEP1; *Kistler et al.*, 2001], the NCEP-DOE reanalysis 2 [NCEP2; *Kanamitsu et al.*, 2002], the NOAA twentieth century reanalysis [20CR; Compo et al. 2010], the wave- and anemometer-based sea surface wind [WAS, Tokinaga and Xie, 2011] data sets, along with the wind stresses that forced the ECMWF Operational reanalysis version S3 [ORA-S3; *Balmaseda et al.*, 2008] and the Simple Ocean Data Assimilation, version 2.1.6 [SODA-2.1.6; *Czeschel et al.*, 2011]. The ORA-S3 and SODA-2.1.6 wind forcing products are not completely independent as both incorporate ERA-40 winds prior to 2002; however, after this period both products transition to different wind products [*Balmaseda et al.*, 2008; *Czeschel et al.*, 2011].

Surface wind stress data are only available for the ORA-S3 and SODA-2.1.6 data sets. For all other datasets the surface winds are converted to wind stresses using the quadratic stress law: $(\tau_x, \tau_y) = C_d \rho_a (U,V) W$; where U, V are the zonal and meridional surface winds respectively, W is the surface wind speed, ρ_a =1.2 kg m^{-3} is a reference atmospheric density, and C_d =1.5e^{-3} is the dimensionless drag coefficient. Wind stress anomalies are computed relative to a mean seasonal cycle based on the 30-year (1979–2008) climatology. Due to the non-linear nature of the stress calculation, the use of monthly winds to calculate stresses may

result in a reduction in wind stress amplitude in the western equatorial Pacific. However, tests with monthly mean stresses calculated from CR20 and ERA-interim daily winds reveal that the results presented here are robust regardless of how the wind stresses are calculated. We also note that in order to focus on processes at ENSO time scales, variability with periods shorter than 8 months were removed from the NCEP2 stresses with a low-pass filter as these stresses contain significantly stronger variability at sub-annual frequencies compared to the other products (not shown).

This study also employs the monthly NINO3.4 index (hereafter N34, namely SST anomalies averaged in the region 5°N-5°S, 90°W-150°W) derived from *Reynolds et al.* [2002]. The SST anomalies are computed relative to a mean seasonal cycle based on the 30-year (1979– 2008) climatology. Note that EP and CP years follow the definition of *McPhaden et al.* [2011], while La Niña years follow the definition of *McPhaden and Zhang* [2009].

3. ENSO winds and SWM experiments

Performing a Principal Component (PC) decomposition on each wind stress product over the tropical Pacific (10°N -10°S and 100°E - 60°W) reveals that each product produces a first PC time series that is largely consistent with N34 region SSTA, including the positive skewness (Figure 1c). The average correlation between this leading PC and N34 SSTA is 0.78 (min = 0.74, max = 0.86). The corresponding spatial patterns, which are obtained by regressing the principal component time series onto the anomalous wind stress anomalies at each spatial location, are broadly consistent across the different products (supplementary Figure S1), with the average spatial correlation of the associated wind stress curl being 0.81 (supplementary Table S1). These spatial patterns, and their average (Figure 1a), feature positive zonal wind anomalies in the western-central Pacific consistent with the first EOF mode of ERA-40 wind stresses shown in *McGregor et al.* [2012]. Given its relative symmetry about the equator; they are hereafter referred to as the ENSO symmetric wind stresses (τ_{sym}).

For all products, the second PC mode changes sign during El Niño events. This is most

105 noticeable during the extreme 1982/83 and 1997/98 El Niño events (Figure 1c). Consistent
106 with the second EOF of ERA-40 wind stresses as presented in *McGregor et al.* [2012] (see
107 their Fig. 2b), the associated regression patterns (supplementary Figure S1), and their average
108 (Figure 1b), are largely meridionally asymmetric and feature a prominent anti-cyclonic
109 circulation in the western north Pacific region consistent with the Philippine Anticyclone
110 [e.g., Wang et al. 2000]. The product-to-product similarity is highlighted by an average spatial
111 correlation of the associated wind stress curl of 0.80 (supplementary Table S1). As the spatial
112 structure of these wind stresses is largely asymmetric about the equator, these are hereafter
113 referred to as the ENSO asymmetric wind stresses (τ_{asym}).

114 As in the *McGregor et al.* [2012] analysis, the linear combination of the τ_{sym} and τ_{asym} wind
115 stresses allows the anomalous ENSO wind stresses to: 1) shift northward in the months prior
116 to the event peak, making the anomalous wind stresses more symmetric about the equator,
117 and 2) shift southward around the peak of the event, ultimately allowing the anomalous wind
118 stresses to become more asymmetric in the months after the event peak (see supplementary
119 Figures S2, S3 and S4). The meridional displacement of winds reconstructed using τ_{sym} and
120 τ_{asym} is largely consistent with observations during EP and CP type El Niño years [e.g.,
121 *Harrison* 1987; *Harrison and Vecchi* 1999; *Vecchi and Harrison* 2003] and La Niña years
122 [e.g., *Lengaigne et al.*, 2006].

123 Three Shallow Water Model (SWM) experiments for each of the six reanalysis products
124 are conducted. Details of the SWM are provided in *McGregor et al.* [2007]. Experiment 1
125 (Exp1) is forced with time-varying τ_{sym} only. Similarly, the second experiment (Exp2) is
126 forced with τ_{asym} only, while the third experiment (hereafter Exp1+2) is forced with
127 anomalous wind stresses reconstructed from both τ_{sym} and τ_{asym} combined. A control
128 simulation for each wind product is also carried out whereby the SWM is forced with the
129 corresponding full anomalous wind stresses. Although the spatial patterns of the τ_{sym} and τ_{asym}
130 wind anomalies are in broad agreement across the products, certain differences do exist

(supplementary Figure S1), as they also do amongst the principal component time series (Fig. 1c). As such, forcing SWM experiments with these different product representations of the τ_{sym} and τ_{asym} wind stresses will provide a gauge of the robustness of the results documented by *McGregor et al.* [2012].

4. Thermocline response

MM2000 have shown that an EOF analysis of observed 20°C isotherm depths reveals an East-West "tilting mode" and a "recharge mode", both of which are consistent with the RDO paradigm [*Jin* 1997]. As expected, τ_{sym} is largely responsible for the East-West "tilting mode" as shown by Exp1 (supplementary Figure S5c). However, we find that although τ_{sym} does induce a "recharge" mode consistent with the RDO theory, it lacks the meridional asymmetry (supplementary Figure S5d) seen in observations (MM2000; see their Figure 3). Our SWM experiments (Exp2) confirm that the meridional shift of ENSO winds, as represented by τ_{asym}, is directly responsible for the meridional asymmetry of the recharge mode in all wind products analyzed here, consistent with the analysis of *Alory and Delcroix* [2002] and *McGregor et al.* [2012] (supplementary Figure S5).

Comparing the changes in the zonally averaged thermocline depth of Exp1+2 and Exp1, which are calculated on the Equator between 100°E-60°W, we find that the added τ_{asym} wind stresses in Exp1+2 reduces the root mean squared error (RMSE) calculated with respect to the control simulation (supplementary Table S3). In 7 out of the 8 products, the added τ_{asym} wind stresses (Exp1+2) act to roughly double the variance of the zonal mean changes in thermocline depth when compared to those of Exp1, whilst in the 8th product (WAS wind stresses) the zonal mean thermocline depth variance is increased by 35% (supplementary Table S3). This confirms that τ_{asym} plays a prominent role in enhancing the τ_{sym} induced zonal mean changes in equatorial heat content [*McGregor et al.*, 2012].

Composites of zonal mean thermocline depth and its changes (identified by $\partial/\partial t$ of zonal mean thermocline depth) during ENSO evolution in the SWM experiments reveal that the

discharge/recharge induced by τ_{asym} generally peaks between Nov-Jan while that due to τ_{sym} generally peaks later during Feb-April (Fig. 2). For EP type events, τ_{asym} (Exp2) produces changes in zonal mean thermocline depth that are comparable in magnitude to those induced by τ_{sym} (Fig. 2a), which on average lead that induced by τ_{sym} (Exp1) by 3 months (Fig. 2d). This suggests that other than enhancing the changes in equatorial heat content during EP El Niño events, the wind stresses associated with τ_{asym} primes the equatorial Pacific for earlier termination than what would otherwise occur with only τ_{sym} forcing. For CP El Niño events (Fig. 2b and e) and La Niña events (Fig. 2c and f), on the other hand, the effect of τ_{asym} on heat content recharge/discharge is relatively small compared to τ_{sym} (Exp1). Since the RDO is fundamentally a linear theory, these results illustrate that it is the recharge/discharge induced by τ_{sym}, and not the effect of τ_{asym}, that is described by the RDO paradigm.

Several studies have identified the southward wind shift, represented here by τ_{asym}, as being due to a non-linear atmospheric response to ENSO SST anomalies [e.g., *Spencer* 2004; *McGregor et al.*, 2012]. Since the magnitude of τ_{sym} is roughly proportional to the strength of ENSO SST anomalies, we would also expect a relationship between the magnitude of τ_{sym} and the extent of τ_{asym} effect on the equatorial heat content. This is illustrated in Fig. 3a, which presents a plot of the Exp2 mean Nov-Jan changes of equatorial heat content versus the corresponding τ_{sym} wind stress component. This plot reveals a clear El Niño/La Niña asymmetry, which is also apparent in the analysis of each product (supplementary Table S2): when the τ_{sym} time series is positive, strong negative correlations exist between τ_{sym} and the Exp2 mean Nov-Jan changes of equatorial heat content that are statistically significant above the 95% level (evaluation of correlation significance level in our study follows that of Sciremammano1979), but no significant correlation is found when the τ_{sym} is negative (supplementary Table S2). This ENSO phase asymmetry highlights the role of τ_{asym} in enhancing heat content discharge during El Niño events, which should ultimately lead to a more abrupt and effective termination with stronger El Niño events, while not having any

183 discernible effect during La Niña.

184 This τ_{asym} ENSO phase asymmetry is distinct from that expected by the RDO theory as
185 depicted by Exp1 (Fig. 3a grey line). Its cause can be traced to the extent of the meridional
186 wind shift (τ_{asym}), which can be represented by the difference between the PC2 value averaged
187 over Aug-Oct and that averaged over Feb-Apr of the following year. Plotting this difference
188 versus τ_{sym} averaged over Nov-Jan (when ENSO peaks) reveals an ENSO phase non-linearity
189 consistent with the τ_{asym} induced equatorial heat content changes (Figure 3b; supplementary
190 Table S2). In fact, there is a strong significant linear relationship between the extent of the
191 meridional wind movement and the recharge/discharge of heat content (Figure 3c).
192 Correlation coefficients between the two time series for each product range from 0.73 to 0.99
193 (an average of 0.9), all of which are statistically significant above the 99% level.

194 To first order, the τ_{asym} induced discharge appears to scale with the intensity of El Niño
195 events as indicated by the magnitude of τ_{sym} (Fig. 3a). However, highlighting EP and CP type
196 El Niño events in Fig. 3 reveals that the τ_{asym} discharge during CP El Niño events appears
197 weaker than that during EP El Niño with similar magnitude of τ_{asym} wind stresses. For each
198 wind product, tests with 1000 bootstrapped means show that the average τ_{asym} discharge
199 during CP events is significantly smaller (at 95% level) than during EP events. It is notable
200 that these differences are still significant (at the 90% level) even when the large magnitude
201 1982/83 and 1997/98 El Niño events are removed from the EP sample. This indicates that
202 factors other than El Niño event magnitude may play a secondary role in determining the
203 prominence of τ_{asym} induced equatorial heat content changes.

204 While all wind products agree on the importance of τ_{asym} wind stress forcing in the changes
205 in equatorial heat content, the large-scale El Niño/La Niña phase asymmetry, and the CP/EP
206 event differences, we note that differences across products are apparent when focusing on
207 individual events (supplementary Figure 6). These differences, which essentially stem from
208 the spread of PC2 time series shown in Fig. 1c, become most important for CP El Niño events

209 (supp. Fig. 6b) where τ_{asym} induced heat content changes are relatively small. For instance,
210 half of the wind products have an average τ_{asym} induced discharge during CP events that is
211 statistically different from zero (above the 90% level), while the remaining half are not. In
212 fact, in this remaining half these tests suggest that there is more than 60% chance that τ_{asym}
213 will recharge equatorial heat content, opposing the RDO type discharge induced by τ_{sym}.

214 **5. Discussion and conclusions**

215 We identify the meridionally quasi-symmetric (PC1, hereafter τ_{sym}) and asymmetric (PC2,
216 hereafter τ_{asym}) wind stresses related to ENSO in eight different wind products (Fig.1a, b) and
217 use SWM experiments to examine their impact on oceanic thermocline changes during
218 different types of ENSO events. The linear combination of τ_{sym} and τ_{asym} allows the
219 anomalous ENSO wind stresses, which are largely symmetric about the equator prior to the
220 ENSO event peak, to shift southward around boreal winter. Further analysis reveals a clear
221 ENSO phase non-linearity in which stronger El Niño events generally lead to a larger
222 magnitude meridional wind movement, while the meridional wind movement during La Niña
223 events remains relatively small regardless of the event magnitude. This asymmetry appears to
224 be distinct from the ENSO phase magnitude asymmetry, where El Niño events are generally
225 larger than La Niña events; as for events of equivalent magnitude the wind shift is clearly
226 stronger during the El Niño phase of the oscillation (Fig. 3b).

227 The reason for this ENSO phase asymmetry is consistent with the explanation put forth for
228 the southward wind shift by *McGregor et al.* [2012], in that the meridional wind movement
229 during El Niño events results from a weakening of the climatological wind speed south of the
230 equator toward the end of the calendar year. The anomalous winds during El Niño events
231 would act to further decrease these climatological wind speeds, potentially enhancing the
232 meridional shift; while during La Niña events the anomalous winds would increase the
233 climatological wind speeds, potentially limiting the southward wind shift.

234 Consistent with the earlier study of *McGregor et al.* [2012] using ERA-40, each of the 8

wind products utilized here show that: i) the variance of zonally-averaged equatorial heat content is increased significantly when τ_{asym} is added to the τ_{sym} wind stress field, ii) τ_{asym} forcing of each wind product is responsible for producing the meridional asymmetry of the Pacific Ocean's recharge mode, and iii) the τ_{asym} induced changes in equatorial heat content occur a few months earlier than the τ_{sym} induced changes. Thus, the second PC mode of equatorial wind stresses (τ_{asym}) plays an integral role in the changes in equatorial Pacific Ocean's heat content and may also lead to the earlier termination of ENSO events, particularly for EP El Niño events. Given the clear anti-cyclonic structure in τ_{asym} (Fig. 1b), east of the Philippines, the potential role of τ_{asym} in the termination of ENSO events is largely consistent with mechanisms proposed in the earlier studies of *Wang et al.* [2000] and *Guilyardi et al.* [2003].

We further show that the τ_{asym} induced changes in equatorial heat content are significantly and linearly related to the extent of the meridional wind shift. As such, the ENSO phase asymmetry in the extent of this meridional wind shift directly leads to an asymmetry in the induced equatorial heat content changes, whereby the discharging effect increases with El Niño amplitude, while the recharging effect remains relatively small regardless of La Niña amplitude. Furthermore, given that equatorial heat content changes are known to prime the equatorial region for the termination of ENSO events, this result implies that asymmetries in the extent of this meridional wind shift may contribute to the observed asymmetry in the duration of El Niño and La Niña events [*Okumura and Deser* 2010] consistent with the findings of *Ohba and Ueda* [2009] and *Okumura et al.* [2011]. However, our study further suggests that the development of the Philippine anticyclone is directly linked to the changes in equatorial heat content, and thus, links the ENSO phase asymmetry with the RDO theory, potentially identifying its underlying mechanism.

Our results also suggest that the average τ_{asym} induced discharge during CP El Niño events is significantly smaller than that seen during EP El Niño events. This is in spite of the fact that

261 there are no significant differences in the average τ_{sym} wind stress magnitude. This result
262 suggests that other factors, such as the spatial structure of the SSTA and the co-variability of
263 Indian Ocean SSTs during EP events (or lack of it during CP type events) [Yuan et al. 2012],
264 may also play a role in determining the prominence of τ_{asym} induced equatorial heat content
265 changes.

266 Finally, we note significant differences between the products are apparent when focusing
267 on individual events. This is most apparent for CP type El Niño events which generally have
268 smaller τ_{asym} induced equatorial heat content changes. These differences suggest that caution
269 needs to be exercised when one attempts to infer the effect of τ_{asym} on equatorial heat content
270 changes during any individual event using a particular wind product. Nevertheless, we have
271 shown that all wind products agree on the importance of the second PC mode (τ_{asym}) of
272 equatorial wind stresses in changing equatorial heat content associated with ENSO, the large
273 scale El Niño/La Niña asymmetry, and the CP/EP El Niño event differences.

274 **Acknowledgments**

275 S. M., M. H. E., A.S. and P.S. are supported by the Australian Research Council. N.R. was
276 funded by the UNSW ECR grant of S.M. and P.S.; M.J.M was supported by NOAA. PMEL
277 Contribution number 3967.

278 **References**

279 Alory, G. and T. Delcroix (2002), Interannual sea level changes and associated mass
280 transports in the tropical Pacific from TOPEX/Poseidon data and linear model results
281 (1964–1999). *J. Geophys. Res.*, **107**, 3153 doi:10.1029/2001JC001067.

282 Ashok, K., S. K. Behera, S. A. Rao, H. Weng, and T. Yamagata (2007), El Niño modoki and
283 its possible teleconnection. *J. Geophys. Res.,* **112**, C11007, doi:10.1029/2006JC003798.

284 Balmaseda, M. A., A. Vidard, and D. L. T. Anderson (2008), The ECMWF Ocean Analysis
285 System: ORA-S3. *Mon. Wea. Rev.*, **136**, 3018-3034, doi:10.1175/2008MWR2433. 1.

286 Compo, G.P., J.S. Whitaker, P.D. Sardeshmukh, N. Matsui, R.J. Allan, X. Yin, B.E. Gleason,

R.S. Vose, G. Rutledge, P. Bessemoulin, S. Brönnimann, M. Brunet, R.I. Crouthamel, A.N. Grant, P.Y. Groisman, P.D. Jones, M. Kruk, A.C. Kruger, G.J. Marshall, M. Maugeri, H.Y. Mok, Ø. Nordli, T.F. Ross, R.M. Trigo, X.L. Wang, S.D. Woodruff, and S.J. Worley, 2011: The Twentieth Century Reanalysis Project. *Quarterly J. Roy. Meteorol. Soc*., **137**, 1-28. DOI: 10.1002/qj.776.

Czeschel, R., L. Stramma, F. U. Schwarzkopf, B. S. Giese, A. Funk, and J. Karstensen (2011), Middepth circulation of the eastern tropical South Pacific and its link to the oxygen minimum zone. *J. Geophys. Res*., **116**, C01015, doi:10.1029/2010JC006565.

Dee, D. P. and S. P. Uppala (2009), Variational bias correction of satellite radiance data in the ERA-Interim reanalysis. *Q. J. Roy. Meteor. Soc.*, **135**, 1830-1841.

Guilyardi, E., P. Delecluse, S. Gualdi and A. Navarra (2003), Mechanisms for ENSO Phase Change in a Coupled GCM. *J. Clim.,* **16**, 1141-1156.

Harrison, D. E. and G. A. Vecchi (1999), On the termination of El Niño. *Geophys. Res. Lett.,* **26**, 1593–1596.

Harrison, D. E. (1987), Monthly mean island surface winds in the central tropical Pacific and El Niño events. *Mon. Wea. Rev.*, **115**, 3133–3145.

Jin, F.-F. (1997), An equatorial ocean recharge paradigm for ENSO. Part I: Conceptual model. *J. Atmos. Science*, **54**, 811–829.

Kanamitsu, M., W. Ebisuzaki, J. Woolen, S. Yang, J. J. Hnilo, M. Fiorino, and G. L. Potter (2002), NCEP-DOE AMIP-II reanalysis. *B. Am. Meteorol. Soc.,* 1631-1643, doi:10.1175/BAMS-83-11-1631.

Kao, H. and J. Yu, 2009: Contrasting Eastern-Pacific and Central Pacific types of ENSO. *J. Clim*., 22, 615–632, doi:10.1175/2008JCLI2309.1.

Kistler, R. and Coauthors (2001), The NCEP-NCAR 50-year reanalysis: Monthly means CDROM and documentation. *B. Am. Meteorol. Soc.,* **82**, 247-268.

Kug, J.-S., F.-F. Jin, and S.-I. An, 2009: Two types of El Niño events: Cold Tongue El Niño

and Warm Pool El Niño. *J. Clim*., **22**, 1499–1515, doi:10.1175/2008JCLI2624.1.

Kug, J.-S., J. Choi, S.-I. An, F.-F. Jin, and A. T. Wittenberg, 2010: Warm pool and cold tongue El Niño events as simulated by the GFDL CM2.1 coupled GCM. *J. Clim.*, **23**, 1226-1239. doi: 10.1175/2009JCLI43293.1.

Lengaigne, M., J. Boulanger, C. Meinkes, and H. Spencer (2006), Influence of the seasonal cycle on the termination of El Niño events in a Coupled General Circulation Model. *J. Clim.*, **19**, 1850–1868.

McGregor, S., N. J. Holbrook, and S. B. Power (2007), Interdecadal sea surface temperature variability in the equatorial Pacific Ocean. Part I: The role of off-equatorial wind stresses and oceanic Rossby waves. *J. Clim.,* **20**, 2643-2658.

McGregor, S., A. Timmermann, N. Schneider, M. F. Stuecker and M. H. England (2012), The effect of the South Pacific Convergence Zone on the termination of El Niño events and the meridional asymmetry of ENSO. *J. Clim*., **25**, 5566-5586, doi:10.1175/JCLI-D-11-00332.1.

McPhaden, M. J., and X. Zhang (2009), Asymmetry in zonal phase propagation of ENSO sea surface temperature anomalies, *Geophys. Res. Lett., 36,* L13703, doi:10.1029/2009GL038774.

McPhaden, M. J., T. Lee, and D. McClurg (2011), El Niño and its relationship to changing background conditions in the tropical Pacific. *Geophys. Res. Lett. 38,* L15709, doi:10.1029/2011GL048275.

Meinen, C. S. and M. J. McPhaden (2000), Observations of Warm Water Volume changes in the equatorial Pacific and their relationship to El Niño and La Niña. *J. Clim.,* **13**, 3551–3559.

Ohba, M., and H. Ueda (2009), Role of Nonlinear Atmospheric Response to SST on the Asymmetric Transition Process of ENSO. *J. Clim.*, **22**, 177–192.

Okumura, Y. M., and C. Deser, (2010), Asymmetry in the Duration of El Niño and La Niña.

339 *J. Clim.*, **23**, 5826-5843, doi:10.1175/2010JCLI3592.1.
340 Okumura, Yuko M., Masamichi Ohba, Clara Deser, Hiroaki Ueda, 2011: A Proposed
341 Mechanism for the Asymmetric Duration of El Niño and La Niña. *J. Climate*, **24**, 3822-
342 3829, doi:10.1175/2011JCLI3999.1
343 Onogi, K. and Coauthors (2007), The JRA-25 reanalysis. *J. Meteorol. Soc. JPN.*, **85**, 369-432.
344 Reynolds, R. W., N. A. Rayner, T. M. Smith, D. C. Stokes, and W. Wang (2002), An
345 improved in situ and satellite SST analysis for climate, *J. Clim*.,**15**, 1609–1625.
346 Sciremammano, F. S., 1979: A suggestion for the presentation of correlations and their
347 significance levels. *J. Phys. Oceanogr.*, **9,** 1273–1276
348 Stein, K., A. Timmermann and N. Schneider (2011), Phase synchronization of ENSO and the
349 annual cycle, Phys. Rev. Lett. 10.1103/PhysRevLett.107.128501.
350 Tokinaga, H. and S.-P. Xie (2011), Wave- and anemometer-based sea surface wind
351 (WASWind) for climate change analysis. Journal of Climate, 24, 267-285,
352 doi:10.1175/2010JCLI3789.1.
353 Vecchi, G. A. and D. E. Harrison (2003), On the termination of the 2002-03 El Niño event.
354 *Geophys. Res. Lett.,* **30** (18), 1964, doi:10.1029/2003GL017564.
355 Vecchi, G. and D. E. Harrison (2006), The termination of the 1997-98 El Niño. Part I:
356 Mechanisms of Oceanic Change. *J. Clim.,* **19**, 2633–2646.
357 Wang, B, R. Wu, and X. Fu, 2000: Pacific–East Asian teleconnection: How does ENSO
358 affect East Asian climate? *J. Climate*, **13**, 1517–1536.
359 Wittenberg, A. T. (2004), Extended wind stress analyses for ENSO, *J. Clim.*, **17**, 2526-2540.
360 Yuan, Y., S. Yang and Z. Zhang (2012), Different Evolutions of the Philippine Sea
361 Anticyclone between the Eastern and Central Pacific El Niño: Possible Effects of Indian
362 Ocean SST, *J. Clim.*, **25**, 7866-7883.

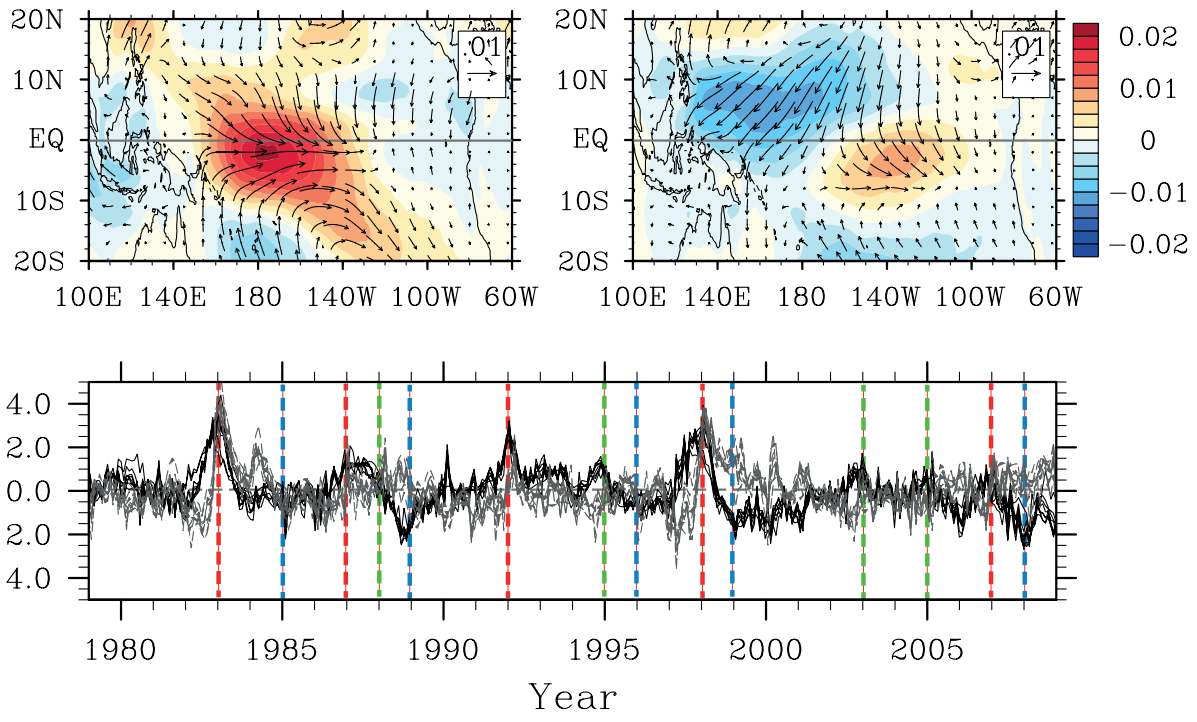

Figure 1: Wind stress patterns associated with (a) τ_{sym}, and (b) τ_{asym} represented as regression coefficients (see text) averaged across the eight products. The zonal component is shaded. c) Time evolution for the τ_{sym} for the eight products is shown in black, while those for τ_{asym} are shown in gray, one for each wind products. The vertical red (green) dashed lines represent the peak December-January for EP (CP) El Niño years, while the vertical blue dashed lines represent the peak December-January for La Niña years. The time series for both τ_{sym} and τ_{asym} across products are highly correlated, with the average 'between product' τ_{sym} correlation being 0.88 (min=0.70 and max=0.98), and the average 'between product' τ_{asym} correlation being 0.80 (min=0.60 and max=0.97).

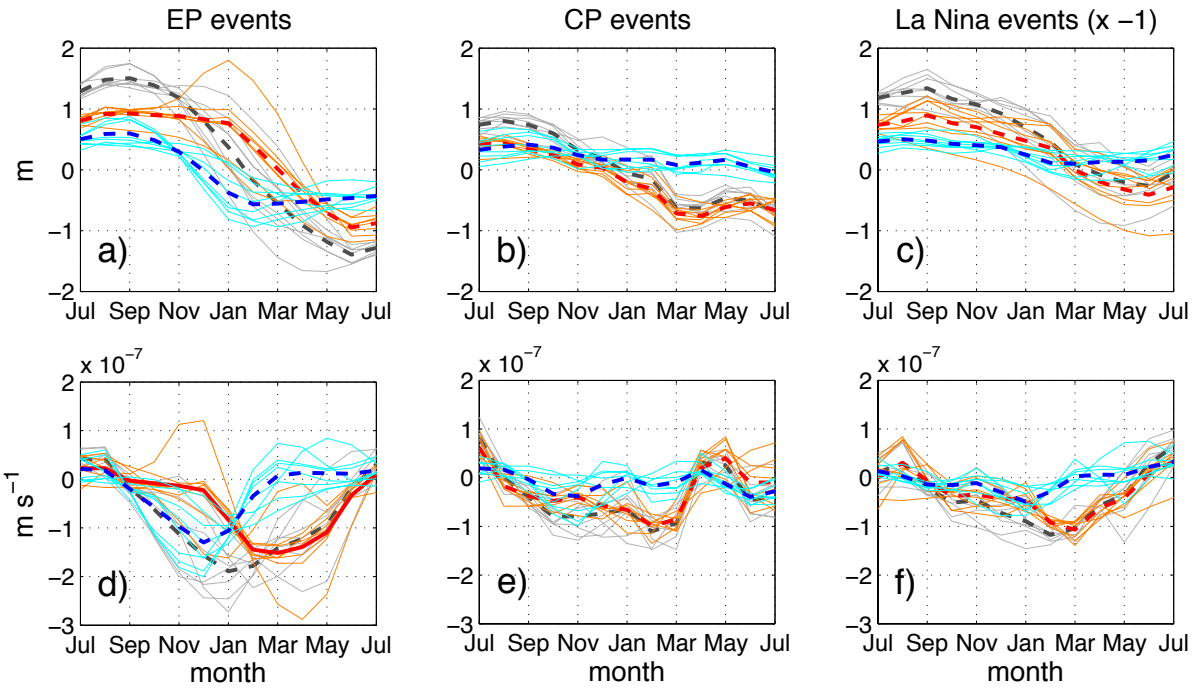

Figure 2: Normalized (against the Exp12 zonal mean thermocline depth) thermocline changes during the different ENSO events in the SWM experiments forced with individual wind products, displayed as composite anomalies of (a)-(c) zonal mean thermocline depth, and (d)-(f) time derivative of zonal mean thermocline depth. The left, middle, and right columns represent EP El Niño, CP El Niño and La Niña composites respectively. In all panels the dashed red, dashed blue, and solid gray lines represent output from Exp1, Exp2, and Exp1+2, respectively. Each of these lines represents the composite means from each individual wind stress product. For easier comparisons, the La Nina composites have been multiplied by -1.

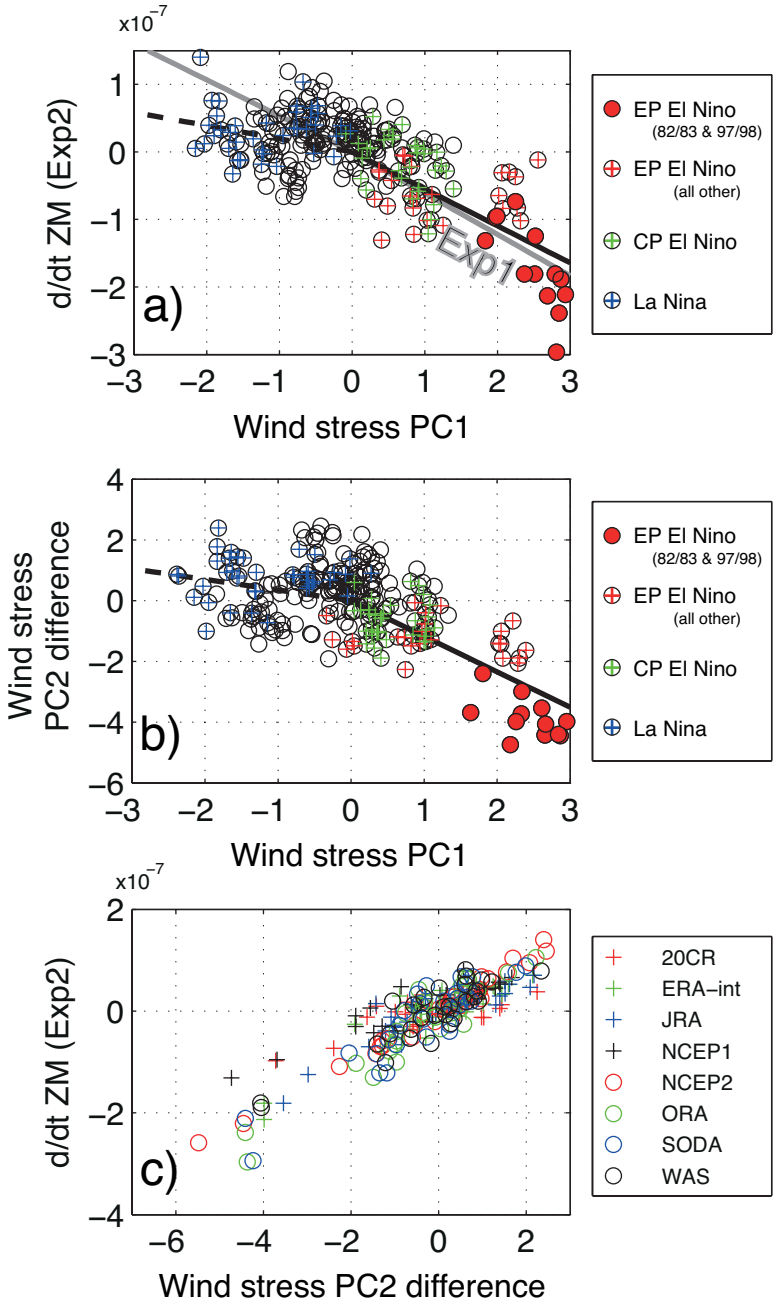

Figure 3: a) Average Nov-Jan discharge of Exp2 equatorial heat content (identified by $\partial/\partial t$ of zonal mean thermocline depth normalized against the Exp1+2 zonal mean thermocline depth) plotted against the corresponding values of PC1 of the equatorial wind stresses for all eight wind products (black circles). The underlying solid black (dashed black) line represents the linear regression slope for positive (negative) PC1 values, while the underlying gray line represents the linear regression slope for both positive and negative PC1 values (calculated separately); b) Each wind product's equatorial wind stress PC2 difference (calculated as the difference between the average Aug-Oct PC2 values and average Feb-Apr PC2 values) plotted against the corresponding Nov-Jan average values of equatorial wind stress PC1 (black circles), again the underlying solid black (dashed black) line represents the linear regression slope for positive (negative) PC1 values. Note that the dashed regression lines indicate none statistically significant correlation coefficients; c) displays each products (see legend) average Nov-Jan discharge of Exp2 equatorial heat content plotted against equatorial wind stress PC2 difference.